A comparative study between dissipative particle dynamics and molecular dynamics for simple- and complex-geometry flows

Eric E. Keaveny, Igor V. Pivkin, Martin Maxey, and George Em Karniadakis[a)]
Division of Applied Mathematics, Brown University, Providence, Rhode Island 02912

(Received 21 October 2004; accepted 14 July 2005; published online 15 September 2005)

The purpose of this study is to compare the results from molecular-dynamics and dissipative particle dynamics (DPD) simulations of Lennard-Jones (LJ) fluid and determine the quantitative effects of DPD coarse graining on flow parameters. We illustrate how to select the conservative force coefficient, the cut-off radius, and the DPD time scale in order to simulate a LJ fluid. To show the effects of coarse graining and establish accuracy in the DPD simulations, we conduct equilibrium simulations, Couette flow simulations, Poiseuille flow simulations, and simulations of flow around a periodic array of square cylinders. For the last flow problem, additional comparisons are performed against continuum simulations based on the spectral/hp element method.
 [DOI: 10.1063/1.2018635]

I. INTRODUCTION

The dissipative particle dynamics (DPD) model consists of particles which correspond to *coarse-grained* entities thus representing molecular clusters rather than individual atoms. The particles move off lattice and interact with each other through a set of prescribed and velocity-dependent forces.[1–3] DPD is potentially a very effective technique in simulating mesoscopic hydrodynamics of simple and complex liquids. Similar to the effort that has been going on with the lattice Boltzmann method (LBM),[4,5] another mesoscopic simulation technique, a systematic verification and validation of DPD, are required to evaluate its accuracy, efficiency, and robustness.

Validation involves comparison with the experimental results. By matching thermodynamic or hydrodynamic properties—for example, the diffusivity of the DPD fluid with water, see Ref. 6, or the surface tension of a binary DPD mixture (e.g., water-benzene, water-CCL_4, water-octane), see Ref. 7—other hydrodynamic DPD-computed parameters can be compared with their corresponding experimental values, thereby demonstrating the validity of the DPD model.

Verification, on the other hand, involves comparison with analytical solutions or other simulation results based on the Navier-Stokes equations. This, for example was done for Couette flow in Ref. 8, for Poiseuille flow in Refs. 9 and 10, and for the lid-driven cavity flow in Ref. 9. Such studies have demonstrated that if the no-slip boundary condition is properly imposed, e.g., see Ref. 9, DPD can indeed reproduce the correct hydrodynamics even for finite Reynolds number flows.

DPD is intrinsically a coarse-graining technique, and thus it is interesting to evaluate the accuracy of DPD simulation results as a function of the number of molecules per DPD particle. The number of molecules per DPD particle is known as the coarse-graining parameter and is denoted by N_m, see Ref. 3. As such, the proper comparison of DPD results should involve a microscopic method, such as molecular dynamics (MD). The question then is what happens as we coarse grain the DPD model, i.e., at values of $N_m > 1$, and what is an upper limit value for acceptable accuracy, for confined systems, i.e., flow systems with solid boundaries.

Unlike a MD simulation where the choice of potential is based on a theoretical model of the physical system to be simulated, a DPD simulation involves potentials of a form independent of the physical system. The DPD potentials do, however, include parameters that need to be properly chosen to provide an accurate approximation of the system. Also, a MD simulation contains a set of units intimately related to the theoretical model. Since, with DPD, the potentials are not given by a physical model, the relation of natural DPD length and time scales to physical units needs to be established.

In the present work, we propose a process of choosing the DPD parameters and determining the DPD length and time scales for different values of N_m, such that the DPD simulations correspond to a MD simulation of a Lennard-Jones (LJ) liquid. The link between the molecular (MD) and mesoscale approach (DPD) is established by determining a thermodynamic property, here the *compressibility modulus*, from MD simulations and adjusting the parameters in the DPD model accordingly. This approach for linking molecular with mesoscopic scales has been proposed by many researchers, e.g., see Ref. 11. After determining the correct parameters and scales, we evaluate the accuracy of the DPD method based on the results obtained from MD simulations and Navier-Stokes solutions. The influence of solid boundaries is typically very strong in DPD simulations, and, to this end, we employ both exact boundary conditions, e.g., the Lees-Edwards boundary conditions,[12] as well as a new set of boundary conditions developed in Ref. 13. The two prototype cases we consider are the plane Poiseuille flow and flow around a periodic array of square cylinders. For the former we also use the analytical Navier-Stokes solution for com-

a)Electronic mail: gk@dam.brown.edu

parison while for the latter we employ spectral/hp element discretizations[14] to obtain highly accurate numerical solutions.

In Sec. II, we provide a brief overview of the basic MD and DPD formulations establishing notation and corresponding units. We then present equilibrium and nonequilibrium simulations to obtain the shear viscosity, which we use in MD and DPD simulations of simple- and complex-geometry domains.

II. MD AND DPD BASICS AND UNITS

In our MD simulations, a system of N particles interact via the pairwise Lennard-Jones potential

$$u_{ij}(r_{ij}) = 4\epsilon\left[\left(\frac{\sigma}{r_{ij}}\right)^{12} - \left(\frac{\sigma}{r_{ij}}\right)^{6}\right]. \tag{1}$$

Therefore, the force on particle i is given by

$$\boldsymbol{F}_i = -\sum_{j\neq i} \boldsymbol{\nabla}_{r_{ij}} u_{ij}(r_{ij}), \tag{2}$$

where r_{ij} is the distance between particle centers, and $\boldsymbol{r}_{ij} = \boldsymbol{r}_i - \boldsymbol{r}_j$.

Once the force on each particle has been determined, the motion of each particle is computed by integrating Newton's second law. In our case, either the fifth-order Gear predictor corrector or the Verlet algorithm[15] performed the time integration. In most of our simulations, we use a modified Lennard-Jones potential

$$u_{ij}^{*} = \begin{cases} u_{ij}(r_{ij}) - u_{ij}(r_{\text{cut}}), & r_{ij} < r_{\text{cut}} \\ 0, & r_{ij} \geqslant r_{\text{cut}} \end{cases} \tag{3}$$

to reduce the computation time. The modified potential allows for the use of a linked list which further reduces the computational cost.

In the nonequilibrium simulations, it is important to control the temperature of the system as we do work on it. For this purpose, we chose to use the extended system Nosé-Hoover thermostat, see Ref. 16. Essentially, this thermostat works by extending the Hamiltonian system to include another variable which moves in accordance with its own potential and scales the velocities of the particles to attain the specified temperature.

In a typical MD simulation of a LJ fluid, the variables and parameters are in terms of reduced units. This set of units is closely linked with the LJ potential, whereby σ is the unit of length, m is the unit of mass, and ϵ is unit of energy. From here, we can define the unit of time, $\tau = (m\sigma^2/\epsilon)^{1/2}$. Further combinations of these parameters provide the reduced units of other variables, see Appendix B of Ref. 15.

Like MD, the motion of the DPD particles is governed by Newton's equations. However, unlike MD, the forces on the particles are not solely given by conservative interactions. For DPD, the force can be broken into three parts

$$\boldsymbol{F}_i = \sum_{j\neq i} (\boldsymbol{F}_{ij}^{C} + \boldsymbol{F}_{ij}^{D} + \boldsymbol{F}_{ij}^{R}), \tag{4}$$

where the C, D, and R stand for conservative, dissipative, and random. For a single-component DPD liquid the forces exerted on particle i by particle j are

$$\boldsymbol{F}_{ij}^{C} = \begin{cases} a(1 - r_{ij}/R_c)\hat{r}_{ij}, & r_{ij} < R_c \\ 0, & r_{ij} \geqslant R_c, \end{cases} \tag{5}$$

$$\boldsymbol{F}_{ij}^{D} = -\gamma w^{D}(r_{ij})(\hat{r}_{ij} \cdot \boldsymbol{v}_{ij})\hat{r}_{ij}, \tag{6}$$

$$\boldsymbol{F}_{ij}^{R} = \sigma_R w^{R}(r_{ij})\theta_{ij}\hat{r}_{ij}, \tag{7}$$

where $\boldsymbol{v}_{ij} = \boldsymbol{v}_i - \boldsymbol{v}_j$ and $\hat{r}_{ij} = \mathbf{r}_{ij}/r_{ij}$. Also, w^D and w^R are weight functions that vanish for $r_{ij} > R_c$, and θ_{ij} is a Gaussian random variable that satisfies $\langle \theta_{ij}(t) \rangle = 0$ and $\langle \theta_{ij}(t)\theta_{kl}(t') \rangle = (\delta_{ik}\delta_{jl} + \delta_{il}\delta_{jk})\delta(t - t')$. In the DPD simulation the cut-off radius R_c is the unit of length. To ensure the Boltzmann distribution is achieved at equilibrium,[2] we require

$$w^{D}(r_{ij}) = [w^{R}(r_{ij})]^2 \text{ and } \sigma_R^2 = 2\gamma k_B T. \tag{8}$$

For simplicity, $w^D(r_{ij})$ is chosen to be $(1 - r_{ij}/R_c)$, which defines the same interaction region as for the conservative forces. Also, $a = a_{ij} = \sqrt{a_i a_j}$, where a_i and a_j are conservative force coefficients for particles i and j, respectively.

A linked list is used to speed up the force computation and the modified velocity Verlet[3] scheme computes the particle motion. Groot and Warren provide a more extensive overview of DPD, especially with regard to integration schemes, in their paper,[3] see also Refs. 17 and 18(a); the latter presents an alternative DPD approach.

III. THE LENNARD-JONES FLUID FOR DPD SIMULATIONS

In Sec. II we provided a brief introduction to the components of MD and DPD simulations. The LJ reduced units of mass, length, and time were presented. In addition, we introduced the relevant DPD parameters a, σ_R, and γ and the DPD length scale R_c. In this section, we provide a detailed description of our proposed strategy for determining the DPD parameters and length scale as they correspond to the simulation of a LJ fluid. This method also includes instructions on determining the DPD time scale, which we refer to as τ_{DPD}, and the mass of a DPD particle, M. With these relations, we can then simulate a LJ liquid using DPD with different levels of coarse-graining N_m.

Our procedures are as follows:

(a) Based on the definition of N_m, we determine $M = N_m m$.
(b) We relate R_c to σ by equating the mass density of the DPD system with that of the MD system.
(c) To find the conservative force coefficient, a, we equate the isothermal compressibility of the DPD system with that of the MD system.
(d) The values of γ and σ_R are chosen based on the temperature of the DPD system, simulation time step, and integration scheme. In addition, γ and σ_R must also satisfy Eq. (8).

(e) By insisting the DPD kinematic viscosity be equal to the MD kinematic viscosity, we extract the DPD time scale, τ_{DPD}.

The method outlined above ensures that the mass density, viscosity, and the compressibility of the DPD simulation are the same as those of the MD system. Specifically, this means the *linear* responses of the pressure to density changes and shear stress to shear rate are the same for both systems. Therefore, this method is suitable for regimes where the flow remains Newtonian and is nearly incompressible. With the isothermal compressibility being both a function of density and temperature, the above method only provides the *local* DPD parameters and unit scales with respect to the point of interest on the phase diagram. Therefore, if one wishes to conduct simulations at two different phase points, the calibration must be performed twice.

Since the current DPD version performs only isothermal simulations, the temperature of the system, $[k_BT]_{\mathrm{DPD}}$, is an input. Usually, $[k_BT]_{\mathrm{DPD}}=1$, but one is not limited to this choice. For example, thoughout this study, we choose $[k_BT]_{\mathrm{DPD}}=0.1$. The choice of DPD temperature manifests itself in the resulting DPD time scale.

A. The DPD cut-off radius

In addition to finding the working parameters for DPD, we need to relate the length scale of DPD, R_c, to σ. This is done by matching the mass densities of the two systems. We denote the dimensional MD number density as ρ_{MD} which has units of σ^{-3}. The DPD number density is denoted by ρ_{DPD} and has units of R_c^{-3}. Therefore, the MD and DPD mass densities are $m\rho_{\mathrm{MD}}$ and $M\rho_{\mathrm{DPD}}$, respectively. In order to equate the two, we must write the DPD expression for mass density in terms of reduced units. Explicitly, the DPD mass density is $N_m m\rho^*_{\mathrm{DPD}}(\sigma/R_c)^3$ where ρ^*_{DPD} has the same numerical value as ρ_{DPD} but units of σ^{-3}. After equating the MD and DPD expressions, we obtain

$$R_c=\left(\frac{N_m\rho^*_{\mathrm{DPD}}}{\rho_{\mathrm{MD}}}\right)^{1/3}\sigma. \tag{9}$$

In all the cases considered $\rho_{\mathrm{MD}}=0.8\sigma^{-3}$ and $\rho_{\mathrm{DPD}}=3.0R_c^{-3}$. The choice of ρ_{DPD} is somewhat arbitrary, provided $\rho_{\mathrm{DPD}}>2.0R_c^{-3}$, see Ref. 3.

B. The conservative force coefficient

To find the value of a in Eq. (5), we follow the process laid out by Groot and Warren[3] and Groot and Rabone,[6] that is, we match the compressibility of the DPD system with that of the MD system. In Ref. 3, the authors, through a series of equilibrium simulations with different values of a and ρ_{DPD}, showed that for sufficiently large number densities, the DPD equation of state computed using the virial Eq. (12), to a good approximation, is given by

$$p=\rho_{\mathrm{DPD}}k_BT+\alpha a\rho^2_{\mathrm{DPD}}, \tag{10}$$

where α was determined to be $\alpha=0.101\pm0.001$. By definition, the isothermal compressibility is $\kappa^{-1}=1/k_BT(\partial p/\partial n)_T$ where n is the number density of actual particles which, in units of R_c^{-3}, is $n=N_m\rho_{\mathrm{DPD}}$. Following Ref. 6, we find

$$\kappa^{-1}=\frac{1}{k_BT}\left(\frac{\partial p}{\partial\rho_{\mathrm{DPD}}}\right)_T\left(\frac{\partial\rho_{\mathrm{DPD}}}{\partial n}\right)=\frac{1}{N_m}\left(1+2\alpha\frac{a\rho_{\mathrm{DPD}}}{k_BT}\right). \tag{11}$$

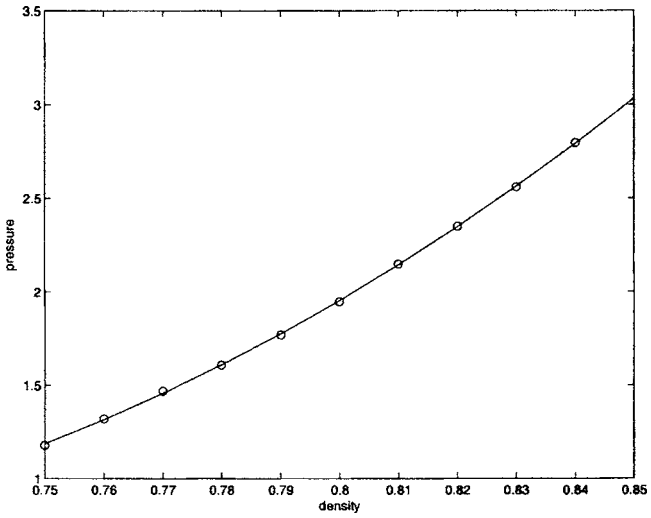

FIG. 1. Pressure vs density obtained from MD simulations for different values of density in order to determine the compressibility of the LJ fluid at $T=1.2\epsilon/k_B$. Here, we find for $\rho_{\mathrm{MD}}=0.8\sigma^{-3}$, $\kappa^{-1}=15.38$.

The above equation provides the necessary relationship between the mesoscopic model parameter and the compressibility of the system. Therefore, with κ^{-1} determined by the MD system, the proper value of the conservative force coefficient can be found.

To obtain κ^{-1}, we conduct equilibrium isothermal MD simulations where the pressure is computed over a range of densities. Like the DPD equilibrium simulations in Ref. 3, the pressure is computed via the internal virial

$$P=\rho k_BT+\frac{1}{6V}\left\langle\sum_{i=1}^{N}\sum_{j=1,j\neq i}^{N}\boldsymbol{r}_{ij}\cdot\boldsymbol{f}_{ij}\right\rangle. \tag{12}$$

In a MD simulation, the pressure is affected by the cut-off radius of the modified LJ potential. We can correct the pressure by using (see Ref. 16)

$$P_{\mathrm{cor}}=P+\frac{16}{3}\pi\rho^2\left[\frac{2}{3}\left(\frac{1}{r_{\mathrm{cut}}}\right)^9-\left(\frac{1}{r_{\mathrm{cut}}}\right)^3\right]. \tag{13}$$

The value of κ^{-1} was found by running equilibrium simulations with $N=2916$ and $r_{\mathrm{cut}}=2.5\sigma$ at $T=1.2\epsilon/k_B$. The pressure was computed for $\rho_{\mathrm{MD}}=0.75\sigma^{-3}$ to $\rho_{\mathrm{MD}}=0.84\sigma^{-3}$. In each instance, the Verlet algorithm was used to advance each system to $t=200\tau$ with $\Delta t=0.005\tau$. The pressure of the system was recorded every time step after $t=10\tau$ and averaged over the 190τ period. The plot of the determined pressure versus density is shown in Fig. 1. The data points are fitted with a quadratic function. By taking the derivative of this function and dividing by the temperature, we find $\kappa^{-1}=15.38$ for $\rho_{\mathrm{MD}}=0.8\sigma^{-3}$. The values of the conservative coefficient a for different levels of the coarse-graining parameter N_m are given by (11) using this value of κ^{-1}.

TABLE I. Equilibrium and Lees-Edwards simulations: DPD and MD simulation parameters. All values are expressed in reduced units even though the results from these simulations determine the time scales. Note that the equilibrium (EQ) MD simulations were performed on a $(11.97\sigma)^3$ domain whereas the Lees-Edwards (LE) MD and all DPD simulations were performed on a $(20.52\sigma)^3$ domain. The symbols used are defined in the text.

	$N_m=1$	$N_m=2$	$N_m=3$	$N_m=4$	$N_m=5$	MD (EQ)	MD (LE)
N	6912	3456	2304	1728	1382	1372	6912
$\Delta t(\tau)$	0.0068	0.013	0.02	0.030	0.04	0.005	0.005
$t_{\text{sim}}(\tau)$	340	1340	3120	5920	10150	1000	1000
$t_{st}(\tau)$	68	134	208	296	406	10	10

C. The random and dissipative force coefficients

The random force coefficient, σ_R, and the dissipative force coefficient, γ, are chosen to yield an efficient and numerically stable DPD simulation that satisfies (8). As the random force increases, the speed at which the system reacts to temperature variations increases.[3] This leads to efficient temperature equilibration. There is, however, an upper limit to one's choice of σ_R. This upper limit is based on the time integration scheme, time step, and temperature. In our DPD simulations, the time integration scheme was the modified velocity Verlet method with parameter $\lambda=0.5$[3], the time step was $\Delta t=0.02\tau_{\text{DPD}}$, and the temperature was $[k_BT]_{\text{DPD}}=0.1$. The results show that temperature deviation diverges rapidly if σ_R is greater than 4.4. For even higher values, the simulation is unstable. Therefore, to have an efficient and stable simulation, we choose $\sigma_R=3.0$. With this value of σ_R, we must have $\gamma=45.0$ to satisfy (8).

D. The DPD time scale

Just as in the case of the length scale, we must relate the time scale of DPD with that of MD. In this case, it is not so clear how the two are related. In Ref. 6 the authors use the diffusion constant of the DPD simulation and matched it to that of the molecule of interest to determine their time scale. They, however, were concerned with the diffusion of water through a membrane. As the Schmidt number (ν/D) for a DPD liquid is lower[18(b)] than that of a real liquid,[3,6] it would be incorrect to use the time scale determined from the diffusion coefficient for viscous processes. Therefore, in our cases where we apply shear to the fluid, we determine our DPD time scale by matching the kinematic viscosities of our systems. We denote the MD kinematic viscosity as ν_{MD} which has units σ^2/τ. For DPD, the kinematic viscosity is written as ν_{DPD} and has units of R_c^2/τ_{DPD}. The DPD viscosity can be rewritten as $\nu^*_{\text{DPD}}(R_c/\sigma)^2\tau/\tau_{\text{DPD}}$ where ν^*_{DPD} has the same numerical value as ν_{DPD}, but units of σ^2/τ. Then, by equating the viscosities, the DPD time scale is given by

$$\tau_{\text{DPD}}=\frac{\nu^*_{\text{DPD}}}{\nu_{\text{MD}}}\left(\frac{R_c}{\sigma}\right)^2\tau. \tag{14}$$

The MD and DPD viscosities are determined by conducting equilibrium and nonequilibrium simulations. The details and results of these simulations are given in Sec. IV.

IV. NUMERICAL SIMULATIONS

We first perform simulations to obtain the shear viscosities of the fluid. Once the visocities have been determined, we perform simulations of plane Poiseuille flow and flow past a periodic array of square cylinders.

A. Equilibrium simulations

We first consider equilibrium simulations to determine the shear viscosities of our MD and DPD systems. We calculate the shear viscosity using the Green-Kubo relation

$$\mu=\frac{V}{k_BT}\int_0^\infty\langle\sigma_{\alpha\beta}(0)\sigma_{\alpha\beta}(t)\rangle dt, \tag{15}$$

where $\sigma_{\alpha\beta}$ is an off-diagonal component of the stress tensor given by the Irving-Kirkwood formula

$$\sigma_{\alpha\beta}=-\frac{1}{V}\left(\sum_{i=1}^{N}mv_{i\alpha}v_{i\beta}+\frac{1}{2}\sum_{j=1,j\neq i}^{N}r_{ij\alpha}f_{ij\beta}\right). \tag{16}$$

To ensure accurate results for the MD simulation, we did not use a cut-off potential. It has been shown, however, that using a cut-off potential can also yield accurate results as long as $r_{cut}>4.5\sigma$.[19]

In Table I we list the simulation parameters and Table II contains the values of the viscosities found via the Green-Kubo relation. In all cases the fully periodic computational domain contained N particles. In reduced units, the DPD and MD simulations correspond to a LJ fluid with $T=1.2\epsilon/k_B$ and $\rho=0.8\sigma^{-3}$. In the MD simulation the domain was $11.97\sigma\times11.97\sigma\times11.97\sigma$ whereas the DPD simulation do-

TABLE II. Shear viscosity results from the Green-Kubo (EQ) and Lees-Edwards (LE) calculations. The values are expressed in terms of DPD units $[M/(R_c\tau_{\text{DPD}})]$. By the method described in the previous section, these values are constructed to be identical (in terms of reduced units) to those found in the MD simulation. The Green-Kubo calculation gave $1.98m/(\sigma\tau)$ as the shear viscosity whereas the Lees-Edwards simulations yielded $1.97m/(\sigma\tau)$.

	$N_m=1$	$N_m=2$	$N_m=3$	$N_m=4$	$N_m=5$
μ (EQ)	1.05	1.31	1.57	1.84	2.16
μ (LE)	1.04	1.31	1.55	1.82	2.15

main was $20.52\sigma \times 20.52\sigma \times 20.52\sigma$. The simulations were run to time $t=t_{\text{sim}}$ to determine the viscosity. The data were collected after a transient time period $t=t_{st}$. For MD, the Verlet scheme was used for the time integration. For the equilibrium simulations, a much smaller domain was used in MD compared to DPD. However, in all other simulations presented, the same size domains were considered.

B. Lees-Edwards simulations

A plane Couette flow generated by Lees-Edwards boundary conditions[12] provides a second way of computing the viscosities of the DPD and MD systems. This is a boundary-free simulation independent of the specific implementation (MD, DPD, etc.) that is employed to impose the no-slip boundary conditions. The shear is imposed in the x direction with the velocity gradient in z direction. For the MD simulations, the shear rates ranged from $0.012\tau^{-1}$ to $0.049\tau^{-1}$, while for all DPD simulations, the shear rates ranged from $0.0015\tau_{\text{DPD}}^{-1}$ to $0.065\tau_{\text{DPD}}^{-1}$. Since a linear velocity profile was observed in each case considered, we can calculate the shear viscosity from the relation

$$\langle \sigma_{xz} \rangle = \mu \frac{\partial u}{\partial z}, \tag{17}$$

where σ_{xz} is given by Eq. (16).

In Table I we list the simulation parameters; the resulting values of the shear viscosity calculated from the nonequilibrium Lees-Edwards simulations are presented in Table II. The agreement with the values obtained through the Green-Kubo relations is good. The simulations were run with N particles in a fully periodic domain. The domain for all simulations was $20.52\sigma \times 20.52\sigma \times 20.52\sigma$. Again $T=1.2\epsilon/k_B T$ and $\rho=0.8\sigma^{-3}$. For the MD simulations, the fifth-order Gear predictor corrector was the time integration scheme, and the Nosé-Hoover thermostat kept the temperature at the desired value. Velocity and stress data were recorded every time step after $t=t_{st}$ to the end of the simulation when $t=t_{\text{sim}}$ and averaged over this period. The z dimension of the domain was divided into 24 bins over which the velocity and shear stress were averaged.

Now that we have established the shear viscosities of our DPD system for different values of N_m, we can, as we have explained in Sec. III, find the appropriate relation between τ_{DPD} and τ for each N_m.

With the time scales established, we turn our attention to nonequilibrium flows in which we can both confirm the method of choosing DPD parameters and units and explore the effects of coarse graining on DPD flow simulations.

C. Poiseuille flow

We aim to compare velocity and stress profiles and examine density fluctuations in MD and DPD Poiseuille flow simulations of a LJ liquid at $T=1.2\epsilon/k_B$ and $\rho=0.8\sigma^{-3}$. Based on our derivations of M, R_c, and τ_{DPD}, the channel sizes and the imposed pressure gradients in the MD and DPD systems are the same.

With the introduction of bounding interfaces, we adjust our simulations to impose the no-slip boundary condition. In MD, this is accomplished by adjusting the potential between the wall particles and the fluid particles. This can be done in two ways. First, see Ref. 20, we can adjust the parameters ϵ_{wf} and σ_{wf} in the LJ potential for wall-fluid particle interactions in addition to adjusting the wall density, ρ_w. Second, see Ref. 21, we can include an additional parameter $0 \leqslant A \leqslant 1$ to multiply the attraction term in the Lennard-Jones potential. Here, we choose the first method since it has been shown to produce a constant slip length as long as the shear rate is sufficiently small.[22] We find that when our walls are constructed of two (100) layers of a fcc lattice, $\sigma_{wf}=\sigma_{ff}$, $\rho_w=\rho_f$, and $\epsilon_{wf}=0.6\epsilon_{ff}$, we have no slip at the wall.

TABLE III. Poiseuille flow: MD and DPD simulation parameters in reduced units. The symbols in the table are defined in the text. The last row is the effective force parameter used to impose the no-slip boundary condition in the DPD simulations, see Ref. 23.

	$N_m=1$	$N_m=3$	$N_m=5$	MD
N_f	8000	2676	1600	8000
N_w	992	440	304	800
$\Delta t(\tau)$	0.0068	0.02	0.04	0.005
$t_{\text{sim}}(\tau)$	340	3120	10 150	15 000
$t_{st}(\tau)$	68	208	406	200
$h(\sigma)$	0.16	0.22	0.27	0.042 75
$a_w/k_B T(1/\sigma)$	2.0224	3.5489	4.8137	

For DPD, the wall are modeled by two layers of equally spaced particles. The density of the wall is equal to that of the fluid. To prevent the penetration of fluid particles into the solid regions, bounce-back reflections are applied at the fluid-solid interface. The conservative force coefficient of the fluid-solid interactions, a_w (see last row in Table III), is adjusted[23] to achieve no-slip conditions at the walls and desired density level in the middle of the channel. Other approaches to impose the no-slip boundary condition have been developed in Ref. 9.

To generate the flow, a force is imposed on each particle. In the MD simulation, this force was chosen to be $0.0091m\sigma/\tau^2$. Therefore, in reduced units, the corresponding force per particle for the DPD simulations was N_m times this value. Based on this imposed force, the viscosity, and the size of our channel, the Reynolds number of the flow is found to be Re=4.6.

The simulation parameters are summarized in Table III. The number of fluid particles is N_f, while the number of wall particles is N_w. As mentioned above, in DPD, the conservative force coefficient of wall particles, a_w, is different from that for fluid particles, a. The fluid occupies the region between the two walls. This region has dimensions of $34.2\sigma \times 34.2\sigma \times 8.55\sigma$, and is periodic in the x and z directions. The fluid domain is subdivided in the y direction into slices of height h where the velocity, density, and stress data are collected. The fifth-order Gear predictor-corrector integration scheme with the Nosé-Hoover thermostat is employed in the MD simulation. The simulations were run to $t=t_{\text{stm}}$ with time step Δt and data were averaged over all steps after time $t=t_{st}$.

In Fig. 2 we plot the resulting streamwise velocity profiles from both MD and DPD simulations—the results are in

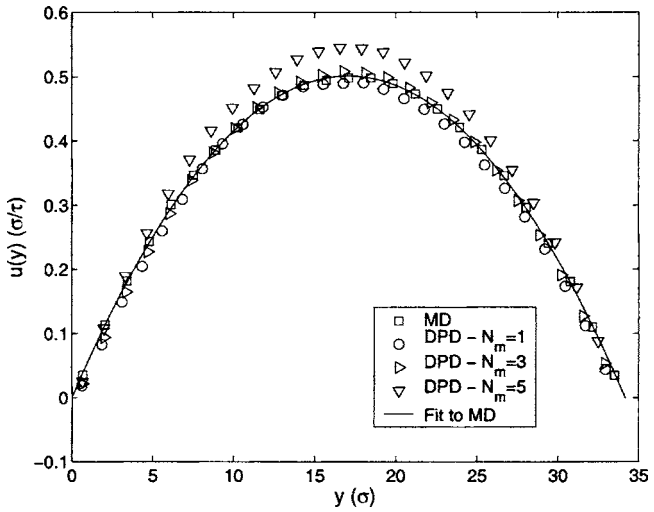

FIG. 2. Velocity profiles of the Poiseuille flow simulations. The determined DPD spatial and temporal scalings are used such that all the data is reported in MD reduced units. The line is the fit to the MD data while the open squares are the MD data, the open circles correspond to DPD/N_m=1, side triangles to DPD/N_m=3, and the inverted triangles to DPD/N_m=5.

reduced units. Three values of coarse graining are included in the plot corresponding to N_m=1, 3, and 5. In Fig. 3 we plot the corresponding shear stress obtained from the two types of simulations. We observe a good agreement between the different simulations both in the velocity profile as well as in the shear stress distribution for N_m=1, 3 but large deviations for N_m=5. Figure 4 shows the density profile across the channel. We observe that the density fluctuations for MD and DPD simulations corresponding to N_m=1 are similar, with the main difference being the large value of the DPD density at the wall. However, as the value of N_m increases the density fluctuations in the DPD simulations also increase, with the N_m=5 case exhibiting very large values at the wall and also inside the flow domain.

We believe that these large density fluctuations associated with N_m=5 lead to the incorrect velocity profile shown in Fig. 2. We found that there are regions of low density which may be as wide as 1.5σ. In these regions the dissipative force is not effective and we obtain high velocity gradients. It may also be that the employed particle-based boundary conditions are not as robust for high values of the conservative force parameter. We note that this value increases when we increase N_m, see (11). In simulations with N_m=5 we observed that the maximum velocity in the center of the channel does not scale linearly with the applied force. For N_m=1 and 3, perfect linearity was observed. In the case just described, we see, specifically, the effects of the microstructure on the continuum dynamics. Therefore, it is important to note that by establishing the link between MD and DPD through bulk thermodynamic quantities, relevant noncontinuum effects may be ignored.

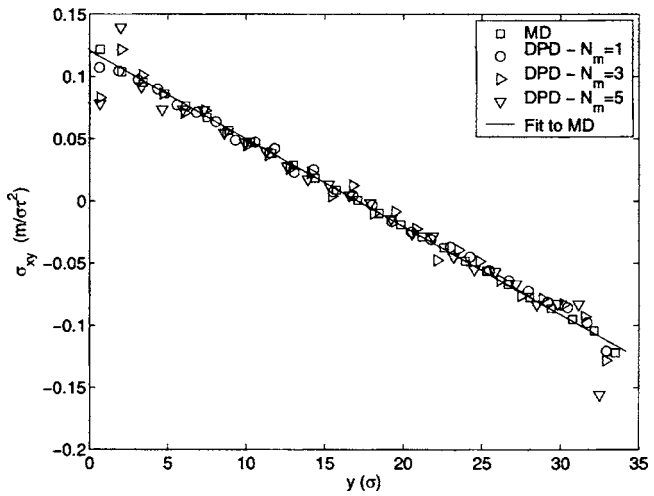

FIG. 3. Corresponding shear stress profiles of the Poiseuille flow simulations. The legend is the same as in the previous figure.

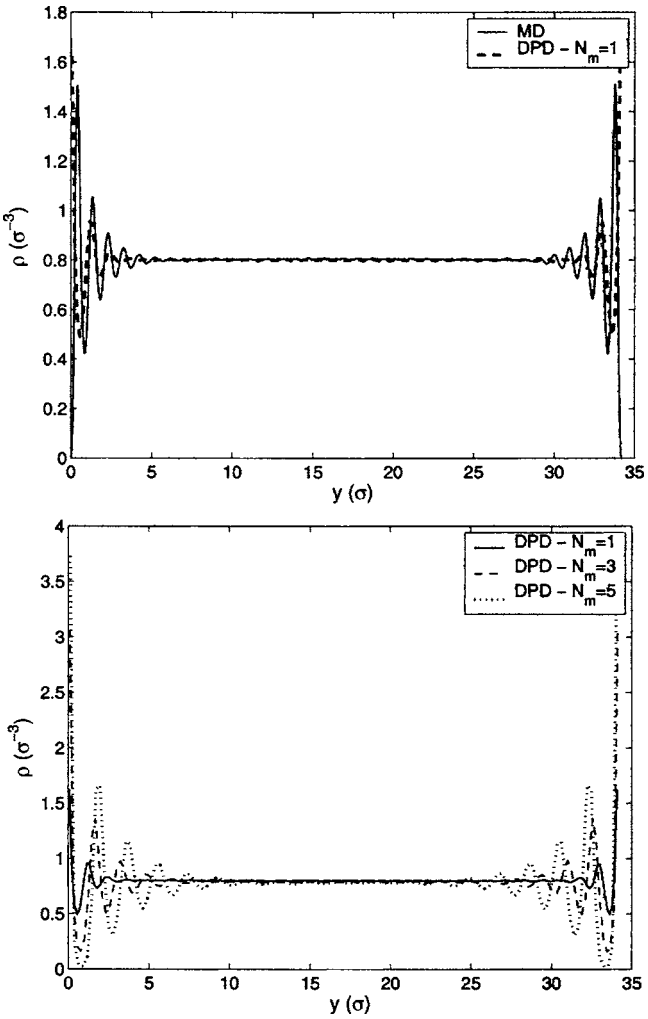

FIG. 4. Density profiles for Poiseuille flow. In the upper plot the MD density is compared against the DPD density for N_m=1. In the lower plot the DPD density profiles are plotted for N_m=1, 3, and 5.

D. Flow past an array of square cylinders

Next we consider flow past a periodic array of square elements and perform MD, DPD, and Navier-Stokes simulations based on spectral/hp element discretization that provides high-order accuracy.[14] The boundary conditions are similar to those employed in the Poiseuille flow (i.e., no slip on the elements and periodicity on all outer boundaries), and the force on each particle is the same in both magnitude and

TABLE IV. Flow past array of square cylinders: simulation parameters for DPD with $N_m=1$, 3 and MD in MD units. Again, the symbols are defined in the text save a_w/k_BT, which is the effective force parameter used to impose the no-slip condition in the DPD simulations, see Ref. 23.

	$N_m=1$	$N_m=3$	MD
N_f	7500	2504	7500
N_w	512	216	500
$\Delta t(\tau)$	0.0068	0.02	0.005
$t_{\text{sim}}(\tau)$	6800	20 800	14 000
$t_{st}(\tau)$	340	1040	250
$h(\sigma)$	0.16	0.22	0.855
$a_w/k_BT(1/\sigma)$	2.0224	3.5489	

direction. Since the speed of sound of the medium is roughly $4.5\sigma/\tau$ and the maximum velocity found is approximately $0.4\sigma/\tau$, the resulting flow is relatively incompressible.

For the simulation of this flow, N_f, N_w, and other parameters are listed in Table IV. The square cylinder has dimensions of $8.55\sigma\times 8.55\sigma\times 8.55\sigma$ and is immersed in a fully periodic domain with dimensions of $34.2\sigma\times 34.2\sigma\times 8.55\sigma$, see Fig. 5. The origin of the reference frame is set as shown in Fig. 5, and the flow is along the x direction. The x and y dimensions were divided into bins of size $h\times h$ over which the data were collected. The simulation was run to time $t=t_{\text{sim}}$ with time step Δt and data were collected after $t=t_{st}$.

For the spectral/hp element simulation, the computations are done in two dimensions using MD units. The kinematic viscosity of fluid is set to $2.475\sigma^2/\tau$ and the external force is $0.0091m\sigma/\tau^2$. The incompressible two-dimensional Navier-Stokes equations are solved using the spectral/hp element solver Nektar.[14] The domain is discretized into 1500 spectral elements of fourth-order polynomial expansion in each element. The simulation is run until a steady state is reached.

We compare the DPD results corresponding to different values of the coarse-graining parameter N_m against the results obtained from the MD simulations and the Navier-Stokes solutions obtained using spectral/hp element discretizations. In Fig. 6, we plot the streamwise and cross-flow velocity components at the centerplane of the domain, and in Fig. 7 we present similar profiles at another location. Also, in Figs. 8 and 9, we plot the corresponding stresses along the y direction. The agreement is good with some small scattering apparent in the stress profiles.

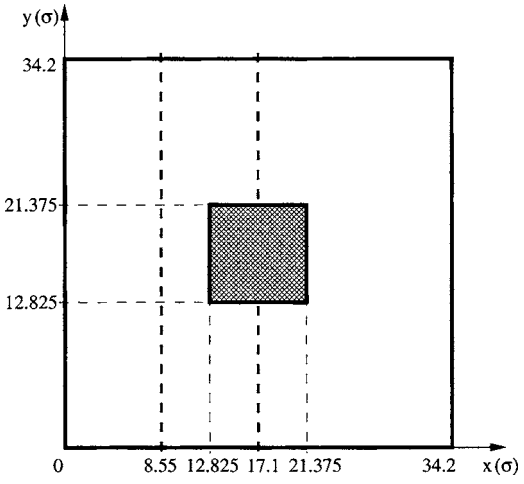

FIG. 5. The geometry of computational domain for flow past array of square cylinders. The dimensions are in MD units. The thick dash lines are the locations where comparisons are performed.

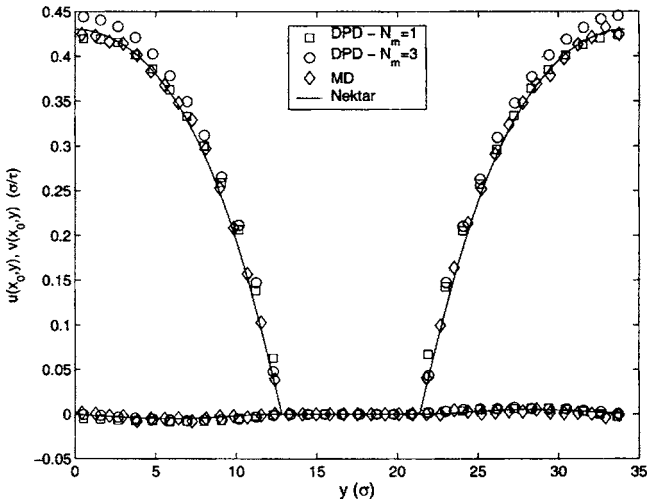

FIG. 6. DPD vs MD: Plots of the u (streamwise velocity) and v (cross-flow velocity) profiles at the center of the square cylinder ($x_0=17.1\sigma$) as given by the DPD and MD simulations.

V. SUMMARY

We have shown that for $N_m<5$ for the channel and for $N_m<3$ for the cylinder array good agreement is established between DPD and MD (and Navier-Stokes) simulations of continuum, no-slip flows in domains approximately 40σ wide. It is important to note that in addition to the flow quantities, we have, by construction, simulated fluids with the same thermodynamic property, i.e., the same dimensionless compressibility. Furthermore, by matching the densities and the viscosities of the MD and DPD systems, we obtained the appropriate length and time scales for a given degree of coarse graining represented by N_m. The validity of these choices is illustrated by the agreement of the scaled DPD data with the MD data, and the Navier-Stokes solutions.

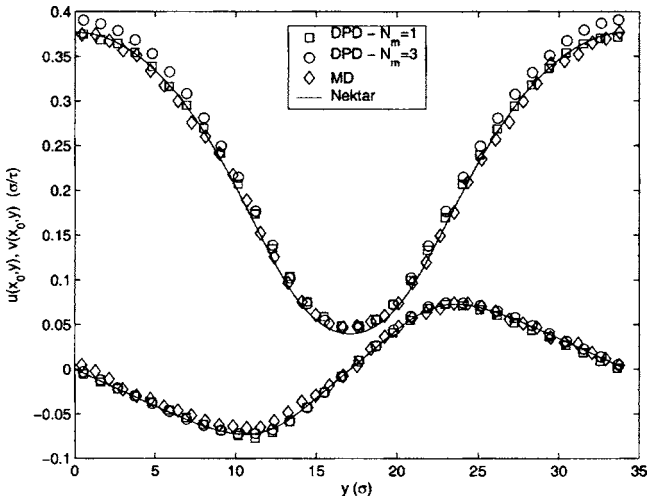

FIG. 7. DPD vs MD and Navier-Stokes: Plots of the u (streamwise velocity) and v (cross-flow velocity) profiles at ($x_0=8.55\sigma$).

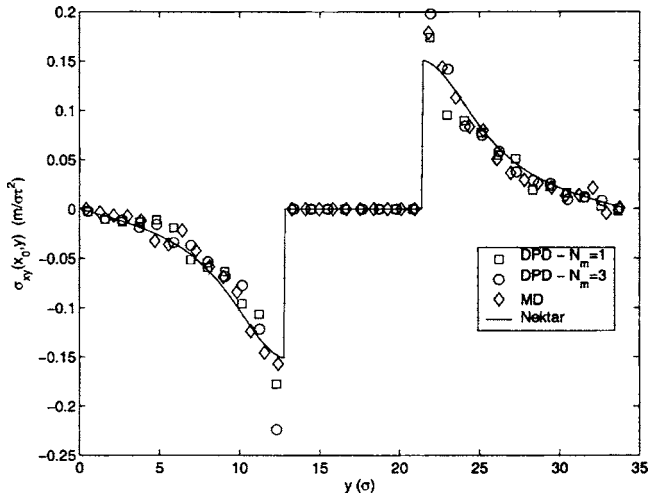

FIG. 8. DPD vs MD and Navier-Stokes: Plots of the σ_{xy} profiles at the center of the square cylinder ($x_0=17.1\sigma$) as given by the DPD, MD and spectral/hp element simulations.

The relatively low upper value of the coarse-graining parameter N_m is somewhat surprising. Moreover, it is intriguing that as the coarse-graining parameter is increased larger density fluctuations occur inside the domain. It is clear that for infinite systems, no such behavior is expected but for confined systems the presence of the boundaries and how the no-slip boundary condition is imposed determine this behavior. It is possible, for example, using the boundary conditions presented in Ref. 9, that the upper values of N_m could be different, although we expect them to be in the same range as the values of $N_m=5$ and 3 obtained here. The problem seems to be with the implementation of DPD procedure and the relative balance of the conservative to the dissipative and random forces. Specifically, as we increase the value of N_m in the current DPD simulations the value of the conservative coefficient increases for a fixed size system, and this has been shown in Ref. 9 to increase the density fluctuations. It is also possible to specifically target the continuum-only behavior of DPD, i.e., not allowing density fluctuations at large values of N_m by developing appropriate boundary conditions, and some preliminary results have been obtained in Ref. 13.

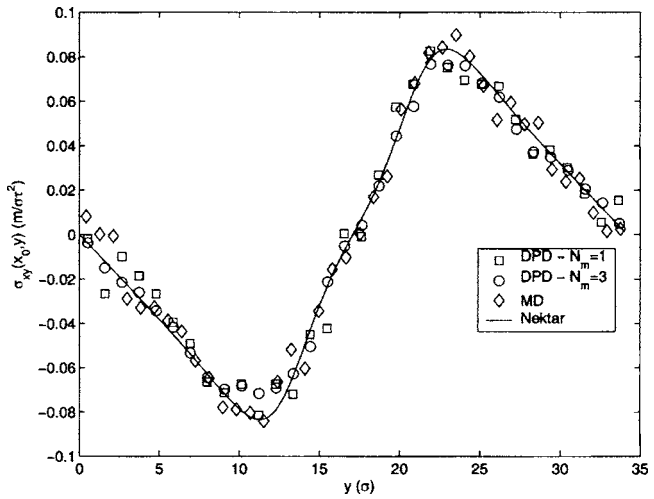

FIG. 9. DPD vs MD and Navier-Stokes: Plots of the σ_{xy} profiles at $x_0=8.55\sigma$.

While we have established agreement between DPD and MD where the continuum solution applies, we have not yet explored the interesting area of the noncontinuum effects, e.g., in submicron-sized channels, where slip may be present.[24] Such a study will require a new procedure to impose slip boundary conditions in DPD based on Maxwellian reflections instead of the bounce-back reflections which are more robust for imposing the no-slip boundary condition, see Ref. 8. A Maxwellian reflection involves particles that are introduced back into the flow with a velocity following a Maxwellian distribution centered around the wall velocity. This issue, however, is not trivial and has not been fully resolved yet even for the lattice Boltzmann method (LBM), see discussions in Refs. 25–27.

Previous studies have been devoted to quantifying the *continuum* resolution of the DPD model, see Ref. 28. This assigns a minimum ratio between the size of an object in a flow to the size of a DPD bead. It would be also of interest to explore the *microscale* resolution of DPD. This could be done by comparing DPD and MD data using different bin sizes. This procedure would assign a quantitative value to the lowest length scale DPD can resolve.

ACKNOWLEDGMENT

This work was supported by NSF (Grant No. CTS-0326720).

[1] P. J. Hoogerburgge and J. M. Koelman, Europhys. Lett. **19**, 155 (1992).
[2] P. Espanol and P. Warren, Europhys. Lett. **30**, 191 (1995).
[3] R. D. Groot and P. B. Warren, J. Chem. Phys. **107**, 4423 (1997).
[4] S. Succi, *The Lattice Boltzmann Equation-For Fluid Dynamics and Beyond* (Oxford University Press, New York, 2001).
[5] S. Chen and G. D. Doolen, Annu. Rev. Phys. Chem. **30**, 329 (1998).
[6] R. D. Groot and K. L. Rabone, Biophys. J. **81**, 25 (2001).
[7] A. Maiti and S. McGrother, J. Chem. Phys. **120**, 1594 (2004).
[8] M. Revenga, I. Zuniga, and P. Espanol, Comput. Phys. Commun. **121-122**, 309 (1999).
[9] S. M. Willemsen, H. C. Hoefsloot, and P. D. Iedema, Int. J. Mod. Phys. C **11**, 881 (2000).
[10] X. Fan, N. Phan Thien, N. Yong, X. Wu, and D. Xu, Phys. Fluids **15**, 11 (2003).
[11] M. Noro, P. Paul, and P. Warren, J. Am. Chem. Soc. **125**, 7190 (2003).
[12] A. W. Lees and S. F. Edwards, J. Phys. C **5**, 1921 (1972).
[13] I. V. Pivkin, Ph.D. thesis, Brown University (2005).
[14] G. Karniadakis, S. Sherwin, *Spectral/Hp Element Methods for CFD* (Oxford University Press, New York, 1999).
[15] M. Allen and D. Tildesley, *Computer Simulation of Liquids* (Clarendon, Oxford, 1994).
[16] D. Frenkel and B. Smit, *Understanding Molecular Simulations: From Algorithms to Applications* Academic, New York, 2002.
[17] P. Nikunen, M. Karttunen, and I. Vattulainen, Comput. Phys. Commun. **153**, 407 (2003).
[18] (a) C. P. Lowe, Europhys. Lett. **47**, 145 (1999); (b) This is not true for the modified DPD version developed by Lowe.
[19] K. Meier, A. Laesecke, and S. Kabelac, J. Chem. Phys. **121**, 3671 (2004).
[20] P. Thompson and M. Robbins, Phys. Rev. A **41**, 6830 (1990).
[21] M. Cieplak, J. Koplik, and J. Banavar, Phys. Rev. Lett. **86**, 803 (2001).
[22] P. Thompson and S. Troian, Nature (London) **389**, 360 (1997).

[23] I. V. Pivkin and G. E. Karniadakis, J. Comput. Phys. **207**, 114 (2005).
[24] G. Karniadakis and A. Beskok, Microflows, Fundamentals and Simulation (Springer, New York, 2001).
[25] B. Li and D. Y. Kwok, Phys. Rev. Lett. **90**, 124502 (2003).
[26] L.-S. Luo, Phys. Rev. Lett. **92**, 139401 (2004).
[27] S. Ansumali and I. V. Karlin, Phys. Rev. E **66**, 026311 (2002).
[28] E. Boek, P. Coveney, H. Lekkererker, and P. van der Schoot, Phys. Rev. E **55**, 3124 (1997.